

Modeling Approach for Reducing Helmholtz Resonance in Submarine Structures

S. Arunajatesan,^{*} and N. Sinha[‡]

Combustion Research and Flow Technology, Inc. (CRAFT Tech)

6210 Keller's Church Road, Pipersville, PA 18947

ajs@craft-tech.com

Phone: 215-766-1520 / Fax: 215-766-1524

This paper discusses CFD technology capable of predicting the occurrence of Helmholtz resonance in surface openings of underwater vehicles. An examination of the numerical issues involved in the prediction is discussed - numerical dissipation, turbulence modeling and their interplay are analyzed through detailed parametric simulations. Further, control of such resonance through the use of passive devices is analyzed. Interesting parallels are observed between resonant flow field behavior in a compressible fluid and the behavior in an incompressible setting with no resonance. This suggests the interesting possibility of controlling resonant flow fields through analysis of corresponding incompressible flow fields.

I. Introduction

Hulls on Naval vessels contain cavities exposed to the ambient flow. The shear flow over these cavities can, under certain conditions, generate resonant oscillations in pressure that can lead to large dynamic loads and loud tonal noise. The dynamic loads can result in structural fatigue, while the radiated resonant tones can propagate very long distances and represents a detection problem. These oscillations occur when resonance occurs between the natural tones of the shear layer over the opening match the natural modes of the cavity itself. Prediction of the flow conditions when this could happen and developing tools for the control of this phenomenon is the subject of this paper.

At present the problem is addressed in two phases. When a problem is identified on a deployed vessel, remedies are developed for that configuration (usually by trial and error or sub-scale model testing). Secondly, an increasing emphasis is being placed on identifying the potential for resonance and avoiding it at the design phase itself. This has led to the use of sophisticated design tools that can adequately model three dimensional complex geometries. The primary requirement on these tools is that they must be capable of handling the complex geometrical shapes encountered in these situations and must be capable of handling the full scale geometries. CFD capabilities in these regards have been demonstrated for simple rectangular cavities (see Refs. 1,2,3,3,5, and the references therein). However, these works have primarily focused on the use of structured CFD codes due to the high order of accuracy achievable and the simplicity of the geometries. The complexity of the geometry under consideration here is more easily handled in an unstructured framework.

The large scales of Navy applications also complicate the search for CFD methods that can accurately simulated shear driven cavity flows. Reynolds-averaged Navier-Stokes (RANS) methods have been shown to be typically too dissipative for accurate resolution of the pressure fluctuations in a shear driven cavity flow (Sinha, et al. ⁶). On the other hand, pure large-eddy simulation (LES), or direct numerical simulations (DNS), such as those of Rowley, et al¹, would be prohibitively expensive for large scale ship geometries, where the flow structures generated far upstream of the cavity must be accurately resolved as they are convected toward the cavity. Therefore, for ship scale applications, a reasonable compromise would appear to be the hybrid RANS/LES approach, originally suggested by Speziale ^{6,7}, in which flow regions where mesh resolution is high enough can sustain LES behavior, while those areas of lesser resolution can resort to RANS behavior.

^{*}Research Scientist, Senior Member AIAA

[‡]Vice-President and Technical Director, Associate Fellow AIAA.

Report Documentation Page

*Form Approved
OMB No. 0704-0188*

Public reporting burden for the collection of information is estimated to average 1 hour per response, including the time for reviewing instructions, searching existing data sources, gathering and maintaining the data needed, and completing and reviewing the collection of information. Send comments regarding this burden estimate or any other aspect of this collection of information, including suggestions for reducing this burden, to Washington Headquarters Services, Directorate for Information Operations and Reports, 1215 Jefferson Davis Highway, Suite 1204, Arlington VA 22202-4302. Respondents should be aware that notwithstanding any other provision of law, no person shall be subject to a penalty for failing to comply with a collection of information if it does not display a currently valid OMB control number.

1. REPORT DATE 2005	2. REPORT TYPE	3. DATES COVERED 00-00-2005 to 00-00-2005	
4. TITLE AND SUBTITLE Modeling Approach for Reducing Helmholtz Resonance in Submarine Structures		5a. CONTRACT NUMBER	
		5b. GRANT NUMBER	
		5c. PROGRAM ELEMENT NUMBER	
6. AUTHOR(S)		5d. PROJECT NUMBER	
		5e. TASK NUMBER	
		5f. WORK UNIT NUMBER	
7. PERFORMING ORGANIZATION NAME(S) AND ADDRESS(ES) Combustion Research and Flow Technology Inc (CRAFT Tech),6210 Keller's Church Road,Pipersville,PA,18947		8. PERFORMING ORGANIZATION REPORT NUMBER	
9. SPONSORING/MONITORING AGENCY NAME(S) AND ADDRESS(ES)		10. SPONSOR/MONITOR'S ACRONYM(S)	
		11. SPONSOR/MONITOR'S REPORT NUMBER(S)	
12. DISTRIBUTION/AVAILABILITY STATEMENT Approved for public release; distribution unlimited			
13. SUPPLEMENTARY NOTES The original document contains color images.			
14. ABSTRACT			
15. SUBJECT TERMS			
16. SECURITY CLASSIFICATION OF:			17. LIMITATION OF ABSTRACT
a. REPORT unclassified	b. ABSTRACT unclassified	c. THIS PAGE unclassified	
			18. NUMBER OF PAGES 12
			19a. NAME OF RESPONSIBLE PERSON

Clearly, there is a need for validated simulation tools capable of modeling Helmholtz resonance prone geometries. The development and validation of such a flow solver is the subject of this paper. The authors have considerable experience in the modeling of shear driven cavity flows in the context of aircraft weapons bay applications.^{1,2,3,3} The use of unstructured flow solver CRUNCH CFD[®] and the hybrid RANS-LES model developed for the prediction of dynamic loads in weapons bays have formed the backbone of much of this work. Here, we present an extension of this work by applying these tools to the prediction of Helmholtz resonance.

II. Physics of Helmholtz Resonator

Excitation of a fully-coupled resonance in a Helmholtz resonator involves two principal components, a source, which is the unstable shear flow along the mouth of the cavity; and, a resonator, in the form of a cavity of defined volume terminated by an open neck or orifice, such that resonance in a Helmholtz mode can occur. A schematic of a typical Helmholtz resonator geometry is shown in Figure 1. An example of a system under Helmholtz resonance is shown in Figure 2. In this figure, velocity vectors and vorticity contours in the shear layer over a deep cavity undergoing resonance in depth mode are shown. The grazing flow is on the bottom while the cavity extends above it. In this coupled state, the large scale oscillations of the shear layer in concert with the oscillations in the depth mode of the cavity are clearly visible.

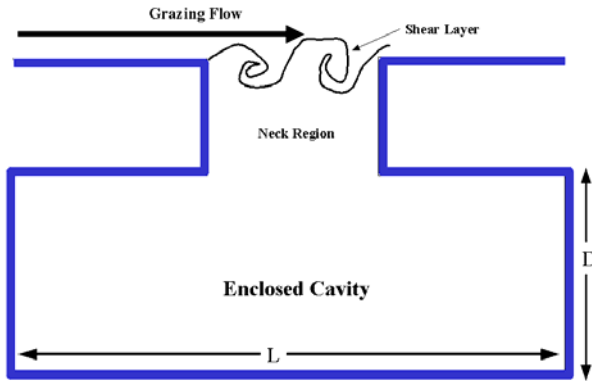


Figure 1. Schematic of a Helmholtz Resonator.

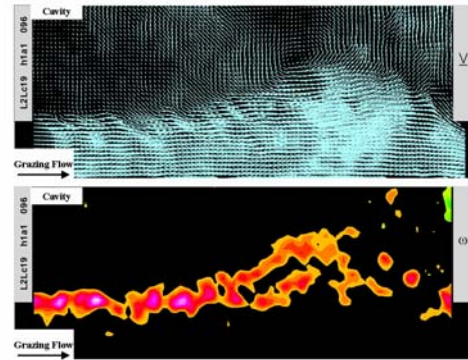


Figure 2. Instantaneous structure of the shear layer along the opening of a deep cavity. Top and bottom images show patterns of velocity and vorticity.

The sequence of events described in the foregoing can fall into two categories. The first category is due to the self-sustained instability of the shear layer. In this mode, there is no coupling with the cavity. The self-sustained oscillations can be very coherent and organized, enabled by a feedback loop along the length of the cavity. The second category of oscillations occurs when this natural instability of the shear layer couples with the natural mode of the cavity. This natural mode can correspond to that driven by pure compressibility of the fluid in the cavity or the natural mode of the structure of the cavity or a combination of both. However, even in the presence of coupling, the features of the first category of oscillations can be clearly identified. Energy methods accounting for acoustic power integral in the shear layer region (e.g., Howe⁸, Nelson⁹) can account for this simultaneous existence of the two categories.

From the above, it is clear that the self-sustained oscillation necessarily precedes and extends into, the resonant oscillation. The opportunity therefore exists to avoid resonant oscillations by effectively attenuating the self-sustained oscillations. Addressing this potential approach is one of the central approaches of this program. From a prediction point of view it is also clear that the prediction of the self-sustaining oscillations is a necessary condition for the accurate prediction of the onset of resonance. Hence, in the present work, the prediction of off-resonance self-sustained oscillations is used as a basis for the selection of the framework suitable for this work. This framework is then used in the predictions of the resonant condition and the controlled flow fields. Comparisons with experimental data are used to validate these predictions and evaluate model performance.

III. Numerical Framework

As mentioned above the CRUNCH CFD[®] code is used in the present work. CRUNCH CFD[®] is a multi-element unstructured flow solver capable of handling all speeds from incompressible to hypersonic with the use of pre-

conditioning to circumvent the stiffness problem at very low Mach numbers. The flow variables are solved for at the vertices using an edge based data-structure using an implicit time marching procedure that employs Newton iterations for second order time accuracy. The major features of the flow solvers are described in other publications^{10, 11} and omitted here for brevity. The main features of the flow solver that are exercised in the present work are the low dissipation variants of the flux procedure, the gradient limiter and the Hybrid RANS-LES model. Only these are described here briefly.

The basic scheme in CRUNCH CFD[®] uses the approximate Reimann solver of Roe for flux construction. The approximate Reimann solver can be overly dissipative when used in an unstructured code. This dissipativeness is partly introduced because the Reimann problem is solved in one dimension normal to the face, ignoring the flow orientation. In the present work this is handled by modifying the flux on the dual face to account for the orientation mismatch between the face normal and the flow direction. Hence, the basic flux computation for the Roe scheme is reformulated as,

$$F_m = \frac{1}{2} \left[F(Q_m^-, \bar{n}_{oi}) + F(Q_m^+, \bar{n}_{oi}) \right] + \frac{1}{2} \alpha \left[\Delta F^-(Q_{Roe}^m, \bar{n}_{oi}) + \Delta F^+(Q_{Roe}^m, \bar{n}_{oi}) \right] \quad (1)$$

$$\alpha = \frac{|\bar{V} \cdot \bar{n}_{oi}|}{|\bar{V}|}$$

This formulation has been tested on simpler shear layer type problems and has shown dramatic reduction in the dissipativeness of the Reimann solver. Another variant in CRUNCH CFD[®] has to do with the gradient limiting procedure employed to achieve a TVD scheme. The baseline limiter used in CRUNCH CFD[®] is that by Barth.¹² This technique limits the gradient of a scalar at any node location based on the extrema of the scalar amongst all the nodes surrounding that node. While this is guaranteed to ensure TVD properties, it can be overly diffusive. The lack of resolution on one edge coming to a node can result in gradient limiting being applied to all the edges coming to that node. Hence, the gradient limiting is modified to an edge-by-edge framework analogous to structured CFD schemes. This has also been shown to make the scheme significantly less diffusive and capable of resolving sharp gradients.¹¹

The hybrid RANS/LES formulation in CRUNCH CFD[®] solves two transport equations, one for sub-grid turbulent kinetic energy, and one for the dissipation rate of turbulent kinetic energy. The dissipation rate is used solely to provide a length scale for RANS regions of the flow. The sub-grid turbulent kinetic energy is then related to an inertial-dissipation range energy spectrum, which is parameterized by the energy containing wave number, k , and the Kolmogorov scale, η . The spectrum is written as:

$$\hat{E}(\hat{k}) = C_\varepsilon \hat{k}_e^{-5/3} \left(\frac{\hat{k}}{\hat{k}_e} \right)^4 \left[1 + \left(\frac{\hat{k}}{\hat{k}_e} \right)^2 \right]^{-17/6} \exp\left(-\frac{3}{2} a \hat{k}^{4/3} \right) \quad (2)$$

where $a = 1.5$, $k = k\eta$, $E = E/(\nu^5 \varepsilon)^{1/4}$, and ν is the kinematic viscosity. In Eqn. (2), k is the wave number, k_e is the energy containing wave number, and C_ε is a constant that calibrates the dissipative range of the spectrum to the local turbulence dissipation rate. The calculated sub-grid kinetic energy is formally related to the energy spectrum as

$$k^{sgs} = \int_{k\Delta}^{\infty} E(k) dk \quad (3)$$

where Δ represents the local mesh resolution. Equation (2) is solved iteratively to determine k_e , which is then the energy containing wave number at that mesh location. Once this is known, the eddy viscosity and the dissipation rates are computed based in this spectrum. More details of this model can be found in Arunajatesan and Sinha.¹

IV. Baseline Helmholtz Resonator Studies

The geometry studied here corresponds to that examined experimentally by Zoccola¹³. A cutout of the geometry illustrating the salient features is shown in Figure 3. The cavity is 19.5 inches long, 36.625 inches wide, and 27.625 inches deep. The opening is 10.5626 inches long and 7 inches wide, and is framed by a 1.5 inch deep combing at

the front and sides, and by a 0.25 inch thick plate at the back. Several flow conditions, corresponding to resonant and non-resonant conditions were studied by Zoccola.¹³ Boundary layer measurements yielding profiles upstream of the cavity opening are available and are used in the calculations to prescribe boundary conditions at the upstream end of the domain. As part of the experiments, the pressure on the wall of the cavity was measured simultaneously with the velocities in the shear layer. The location of the pressure tap and the grid used for the measurement of the velocities in the shear layer are shown in Figure 4.

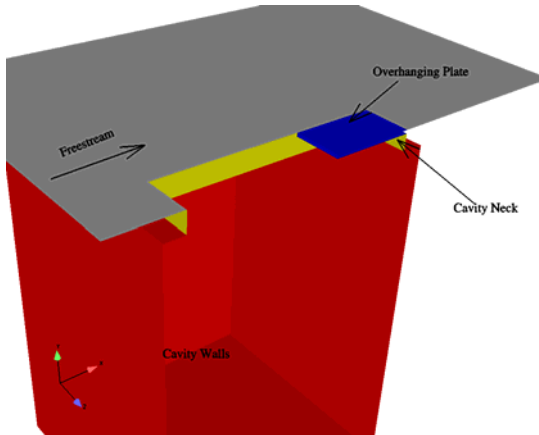


Figure 3. Cutout showing the Helmholtz resonator geometry studied here.

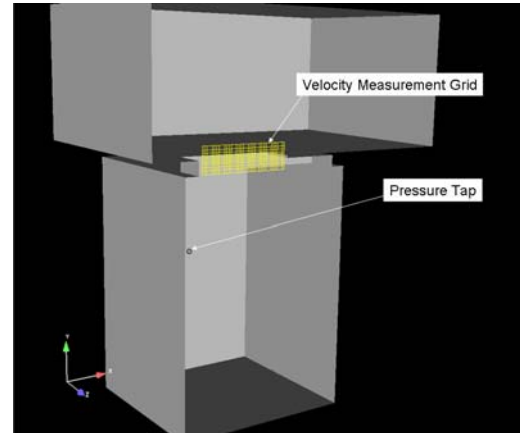


Figure 4. Measurement locations.

A. Non-Resonant Flow

As mentioned earlier, the simulations of the non-resonant conditions were carried out first to identify the simulation parameters. The flow speed was 30 ft/s with a boundary layer momentum thickness of 0.01m at the cavity lip. A computational mesh containing 3.5 million cells (1 million vertices), generated using SolidMesh grid generator was used.

Four calculations have been carried out, exercising various flow solver options to test the fidelity requirements for modeling the non-resonant case. These four cases are listed in Table 1 and examine two different options for the numerical scheme, gradient limiter and turbulence model, each. These are factors that affect the dissipativeness of the numerical scheme and can have a profound impact on the onset of shear layer modes.

Table 1. Cases studied in the self-excited, non-resonant case

Case	Numerical Scheme	Gradient Limiter	Turbulence Model
C1	Baseline	Baseline	Baseline
C2	Baseline	Low-Dissipation	Baseline
C3	Low-Dissipation	Low-Dissipation	Baseline
C4	Baseline	Low-Dissipation	MILES (no-model)

The first calculation uses the baseline limiter (labeled Barth limiter in the figure below) in CRUNCH CFD[®], wherein the gradients at a node are limited so as not to exceed the extrema computed from all its nearest neighbors. In the second calculation, a less dissipative limiter that limits the gradients on an edge-by-edge basis is used instead. Calculations using low dissipation flux scheme in CRUNCH CFD[®] are also carried out in case C3 to see if any interaction exists between the scheme and limiter that is affecting the results. Finally, the dissipation introduced by the turbulence model and its interaction with the scheme and the limiter is isolated by eliminating the model and carrying out the simulations in a no-model mode – also known as the MILES approach in the literature.

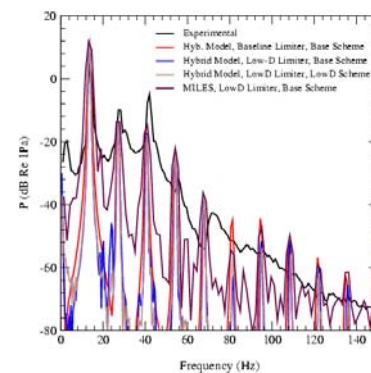


Figure 5. Comparison of the FFTs of wall pressure in the cavity.

Figure 5 shows a comparison of FFTs of the wall pressure in the cavity. The calculations are able to predict the modes dominant in the flow field very accurately. The first mode corresponds to the most dominant shear layer rollup process. The higher modes are the harmonics of this dominant frequency. The amplitude associated with this frequency is also very well captured by the calculations. The amplitude of the second and third modes are slightly under-predicted by the calculations. The interesting aspect of this plot is that very little difference is seen in the predictions offered by the four cases.

A comparison of the mean and rms streamwise velocity measurements along with the Reynolds stresses on the grid shown in Figure 4 is presented for the four cases in Figure 6. Here, several differences are visible in the predictions from the four cases.

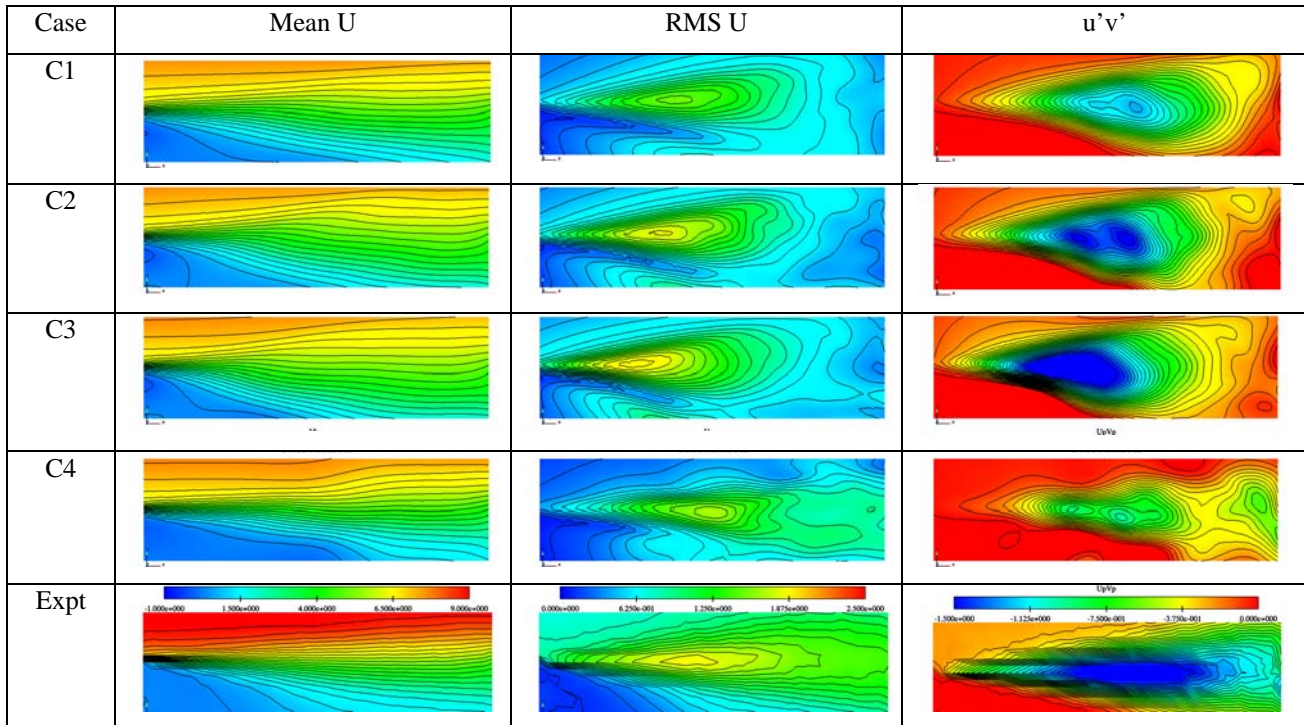


Figure 6. Comparison of the velocity field statistics from the calculations and the experiments.

The mean velocity gradients are seen to be slightly greater in the experimental contours at the upstream locations than in the calculations. This could imply that the mean velocity profile approximation for this case (obtained by scaling the profile for the resonant case) was not a very good one. However, the rest of the mean flow predictions seem in reasonable agreement with experimental measurements. The RMS profiles, for all the cases seem to be slightly shifted upstream, though the prediction for the case C4 seems to do slightly better than the other cases. The intensity of the rms fluctuations at the aft end of the opening, however are uniformly under predicted, indicating that as the vortex roll-up impinges on the plate at the aft end, considerable dissipation has set in. A comparison of the Reynolds stress seems to show the maximum variations between the cases. The Cases C1 and C4 seem to very poorly predict the peak in the Reynolds stresses. Case C2 is slightly better; however, Case C3 seems to do an adequate job of capturing the peak in the Reynolds stress.

The failure of the case C4 to predict the Reynolds stresses indicates that a turbulence model is absolutely necessary for the simulations. The results from Case 1, and again the poor predictions of the Reynolds stresses, seem to indicate that the use of a low dissipation limiter is likely to improve predictions. Comparison of the predictions from cases C2 and C3 indicate that the use of a low dissipation scheme in conjunction with the low dissipation limiter yields the best predictions of the Reynolds stresses. Hence it is concluded that this is the best suitable simulation framework for modeling non-resonant self-excited flow conditions of the cavity flow.

B. Resonant Flow

The resonant flow velocity was 99.6 ft/s, the upstream boundary layer had a momentum thickness of 0.01m. The mesh used for the resonant calculations was the same as the one used for the non-resonant flow field calculations.

In order to examine the effect of the resonance on the vorticity field in the shear layer, contours of the spanwise vorticity for both the resonant and non-resonant cases are shown in Figure 7. Here, we clearly see the large scale oscillations in the shear layer. As in the baseline case, the shear layer is dominated by the presence of only one large scale vortex. However, a comparison of the analogous plots from the non-resonant case reveals that the vortex strength is larger in the case of the resonating flow field. This is to be expected, since the supporting shear to sustain this vorticity is greater due to the higher free stream velocity condition during resonance.

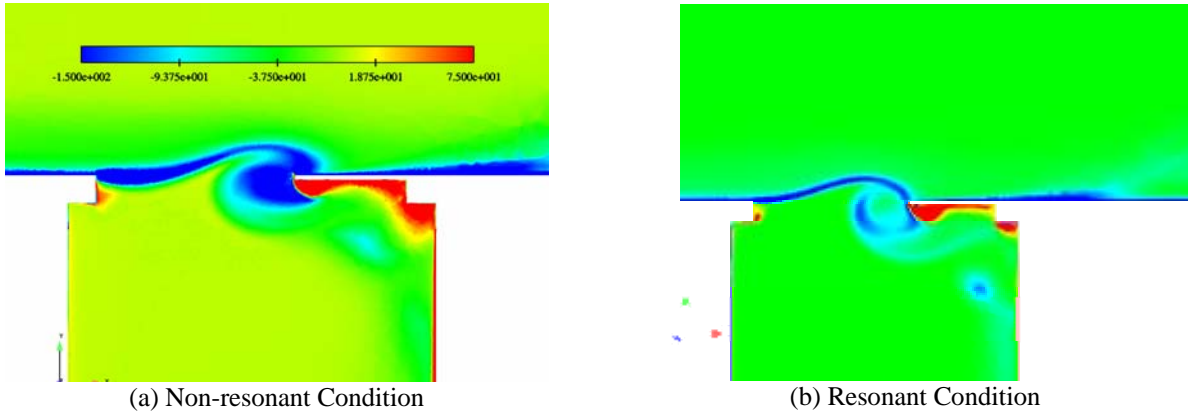


Figure 7. Instantaneous Vorticity Contours from the baseline cases.

As in the non-resonant case, the primary metric of interest in these calculations is the predictions of the cavity wall pressure histories. A comparison of the experimentally measured wall pressure FFT and the computed pressure FFT is shown in Figure 8. The sampling rate used in the experiments is 1ms while that used in the calculations is 0.2ms. The experimental FFTs are obtained by ensemble averaging 32 non-overlapping 1K segments of data. The simulation results are obtained by averaging 16 non-overlapping 2K segments of data.

The comparison shown in Figure 8 also shows results from a companion calculation that did not use a turbulence model. The reason for performing this calculation was that in the non-resonant case, the non-model case gave reasonable predictions. The comparisons show that the simulations are able to predict the surface pressure spectra reasonably well. The frequency and amplitude of the first four modes are very accurately predicted. Again it is seen that the background levels of the pressure FFT are slightly under predicted – the background levels are however, very low in amplitude and are hence not very significant. The prediction of the frequencies along with the prediction of the amplitudes of the energy containing modes implies that the simulation is predicting the occurrence of resonance very well.

As in the baseline case, the Reynolds stresses computed from the simulations were compared with the Reynolds stresses measured from Zoccola’s experiments. These comparisons are shown in Figure 9 for the mean streamwise velocity field, the rms streamwise velocity fluctuations and the Reynolds stress term. Here we see that the predictions of the velocity field in both the mean and rms sense are in reasonable agreement with the experimental measurements. However, significant differences are seen in the predictions of the Reynolds stresses. The reasons for this difference are unclear at this point, especially in light of the excellent agreement between the wall pressure measurements and the predictions. One possible explanation for this is that the frequencies contributing to the pressure oscillations are not the same as those contributing to the Reynolds stresses and hence the prediction of the latter does not necessarily affect the prediction of the wall pressure. In this case the greater pressure and velocity fluctuations indicate that energy leakage from the turbulent flow field could be contaminating the Reynolds stress distributions, thereby pointing towards better resolution requirements for these calculations. Further investigation is required to obtain a better understanding of this discrepancy in the predictions.

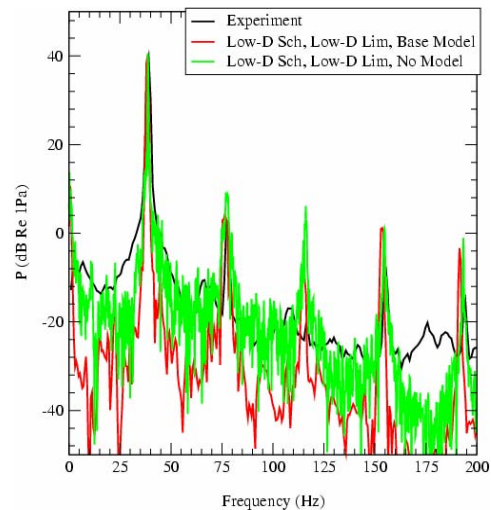


Figure 8. Comparison of the wall pressure FFTs for the resonant case.

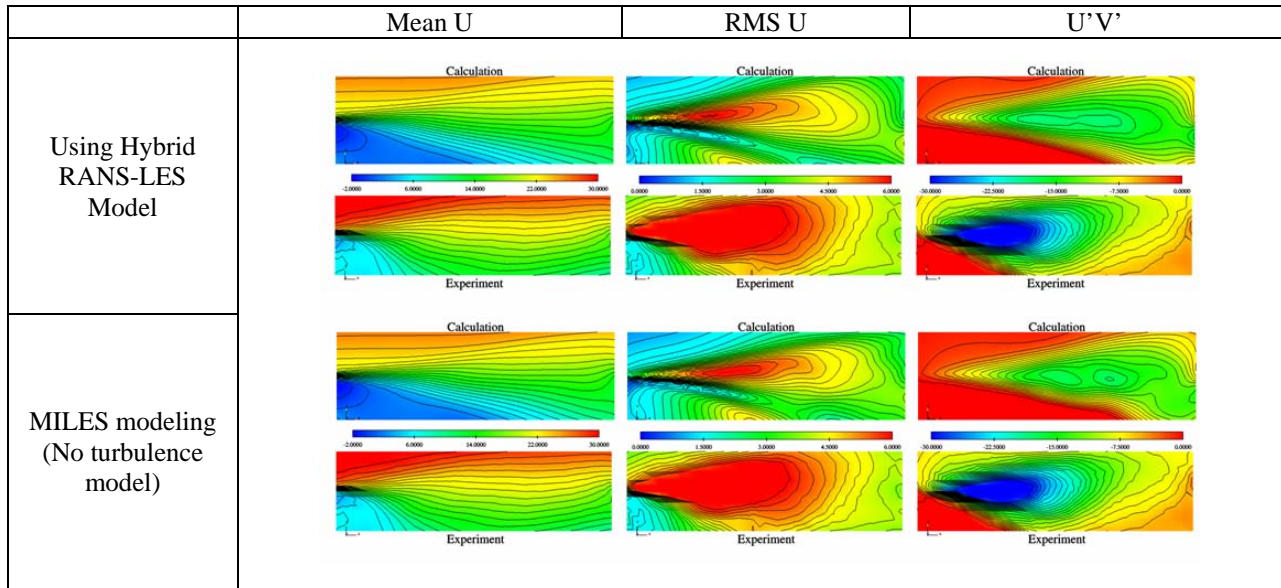


Figure 9. Comparison of the flow field statistics computed from the two cases with the experimentally measured statistics.

The calculations and the simulation results described above show that the CRUNCH CFD[®] solver is capable of computing the flow field associated with Helmholtz resonators reasonably well. The flow physics such as, the behavior of the shear layer, the dependence of the flow field on the free stream velocity and the upstream boundary layer are captured reasonably well. The surface pressure spectra in the cavity compare very well with measurements, both, at resonance and off resonance conditions. This gives us confidence that the solver is well suited to studying the physics associated with these configurations and for the development control concepts for the mitigation of resonance in these structures.

V. Helmholtz Resonator With Slotted Opening

As discussed earlier, one of the potential applications for this flow solver is its use in designing resonance suppression strategies. One common control strategy employed in Naval vessels is the use of slats across the cavity opening, in the hope of destroying the coherence of the shear layer. However, in several cases this approach does not work very well. In order to examine the physics of the underlying flow field associated with such a control concept, a configuration employing these slats was examined by Zoccola.¹³ This configuration was also studied computationally to both, validate the flow solver for controlled configurations and to supplement understanding of the flow field obtained from the experiments.

A schematic of the configuration is shown in Figure 10. The flow field conditions correspond to the resonant flow conditions described earlier. The upstream boundary layer is also identical to the resonant case. The mesh used in these calculations is shown in Figure 11. Prism layers were generated over the slats to resolve the viscous flow region around the slats accurately. The mesh contains approximately 10 million cells and over 3.2million nodes. This mesh was also generated using SolidMesh grid generator. The measurements again comprised of the wall pressure measurements and the simultaneous shear layer velocity measurement at the same locations as the baseline cases.

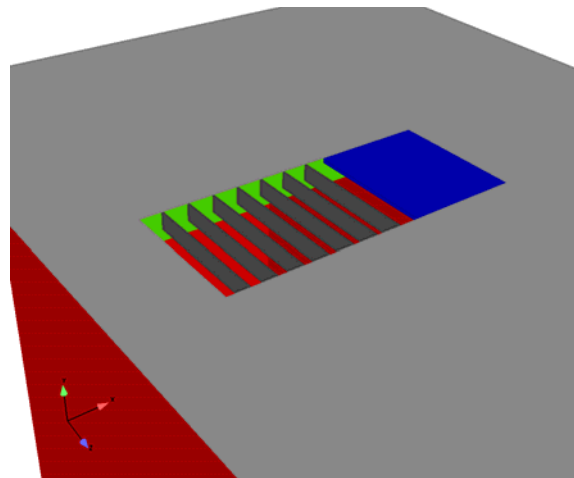


Figure 10. Schematic of the Helmholtz resonator with a slotted opening.

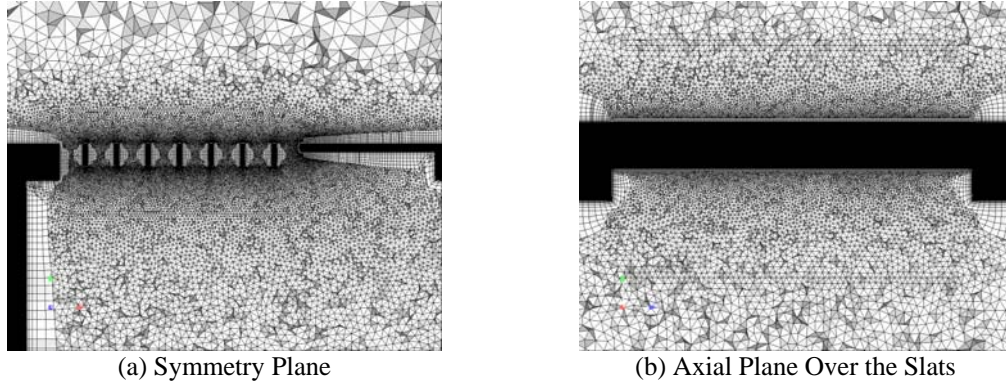


Figure 11. Mesh used in the slotted opening resonator studies.

A visualization of the flow field past the slotted opening is shown in Figure 12. Here, an instantaneous snapshot of stream wise velocity contours on the symmetry plane in the shear layer region is shown. The image shows the existence of oscillatory behavior analogous to the one seen in the resonant open case (Figure 13). The flow field in the neck region is clearly modified by the presence of the slats and the shear layer oscillation does not seem to dip as strongly into the cavity due to their presence. The shear layer oscillations in the region above the neck are seen to be very similar to that in the open resonant case.

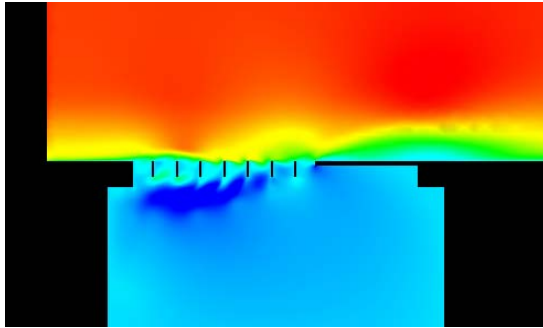


Figure 12. Instantaneous snapshots of the velocity field in the shear layer region for the slotted resonator case.

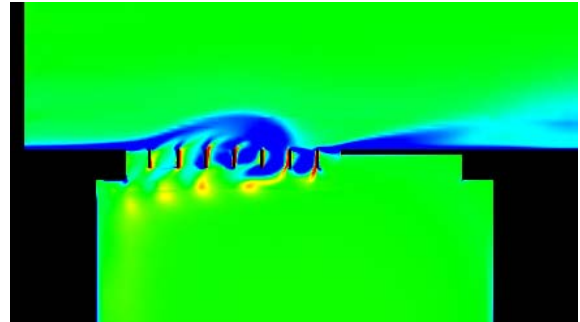


Figure 13. Instantaneous snapshots of the spanwise vorticity in the shear layer region for the slotted Helmholtz resonator.

Visualization of the spanwise vorticity field in this same region and at the same time instant is shown in Figure 13. The presence of the large scale rollup analogous to the resonant case is clearly visible here. The presence of the slats causes the shedding of small vortices rotating counter to the large scale rollup beneath the slats. However, the presence of the slats themselves does not seem to impede the development of the large scale vortex itself. While the position of the large scale rollup in this case is slightly shifted towards the free stream, the intensity is comparable to the resonant open cavity case. The presence of this large scale vortex and its comparable intensity levels (compared to be open resonant case) indicates that the pressure fluctuation levels in the cavity are probably not greatly diminished.

Wall pressure FFT comparisons with data are shown in Figure 14. The conclusions based on observations of the flow field contours are verified in this plot. Here, we see that the amplitude and frequency of the pressure fluctuations are very similar to that obtained from the resonant open cavity case. Comparison of these curves with that from Figure 8 shows that the frequency of the oscillations is not changed significantly. This shows that the resonance with the cavity modes is not altered, although it is possible that the manifested effects of this resonance on the details of the shear layer development itself may be different from the open resonant case.

The comparison in Figure 14 also shows that the numerical model is able to capture this effect very well. The first three modes are very accurately captured. The amplitude of the fourth mode is over predicted. Examination of this frequency with Strouhal numbers associated with various geometrical features of the configuration does not reveal any association with a geometrical feature. The fifth mode however, corresponds to a Strouhal number of 0.2 based on the slot width and free stream velocity. But overall agreement with the experimental spectrum is seen to be very good. It is interesting to note that the broadband levels are also in reasonable agreement for this configuration.

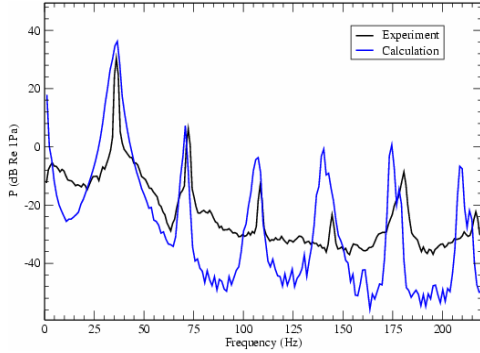


Figure 14. Comparison of the computed wall pressure spectrum with experimentally measured spectrum.

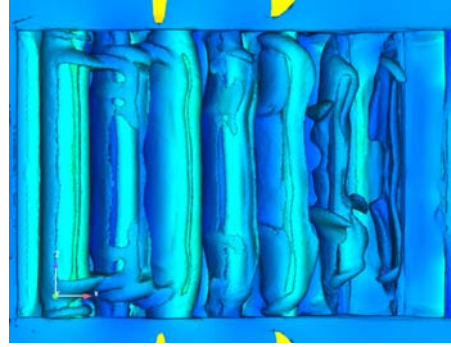


Figure 15. Vorticity magnitude iso-surfaces over the slot region in the slotted opening resonator case.

A reason for existence of this large-scale vortex can be seen in Figure 15. Here the instantaneous vorticity magnitude iso-surface is shown over the slats in the cavity opening. From this figure it can be seen that the flow field is largely two dimensional. In fact, the presence of the spanwise slats seems to promote the two-dimensionality in the slots region.

In order to understand the effects of the slots on the shear layer flow field, detailed visualization of the flow vectors in the slot region was carried out. These vectors are plotted in Figure 16. Also shown in this figure are profiles of the y component of the velocity through the slots. The figures again span one cycle of oscillation and are picked to be roughly one quarter time period apart. From the vector plots it is seen that the flow within the slots is also very rich in flow structure. A very definite cyclical behavior is seen in the evolution of the slot flow. The flow cycle in one slot is at a fixed phase lag behind the low evolution in the slot in front of it and also has a very definite phase relationship to the evolution of the large scale vortex over the entire opening. These relationships are more clearly visible in the profile plots in the right hand side column. The existence of a large scale wave, spanning the length of the cavity opening is clearly visible. Also seen is the clear phase relationship between the propagation of

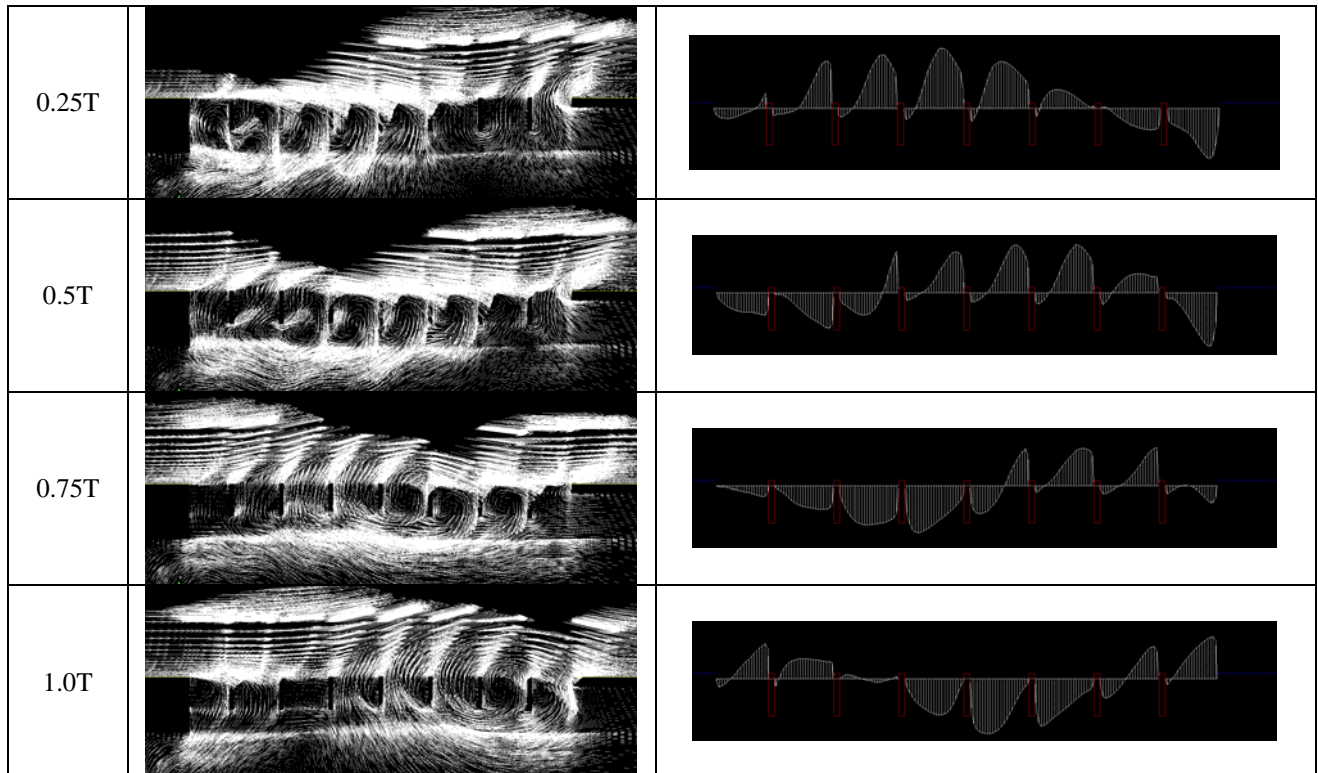


Figure 16. Time series of the velocity vectors and vertical slot velocities in the slot region of the slotted opening resonator.

this wave (signifying the evolution of the large scale vortex in the vector plots) and the flow in the individual slots. The oscillatory flow in the slots rise and fall in accordance with the wave shape spanning the opening. An interesting feature of this flow field is the magnitude of the oscillatory flow in the slots – the amplitude of the oscillations is seen to be more or less uniform across all the slots. This is an evidence of the existence of resonance with the cavity natural modes. The large acoustic energy production across the entire opening resulting from this coupling causes uniformly large ejection and injection velocities across all the slots.

VI. Incompressible Flow Past A Slotted Plate

A configuration similar to the one studied in the previous section was also examined by Rockwell and co-workers^{Error! Reference source not found.} at Lehigh universities to try and understand the physics of the behavior of flow past slotted plates. This was motivated by observations of increased oscillatory behavior in such configurations in the presence of the slots compared to the flow field without the slots. To understand the reasons for this occurrence, they undertook experiments in a water tunnel facility at Lehigh University. Following the observations from the controlled Helmholtz resonator, it was decided to study this flow field numerically, both to provide another validation point and to examine if the phenomenon is hydrodynamic in nature or is governed by the existence of resonance in the Helmholtz resonator.

The configuration studied is schematically shown in Figure 17. The experiments were carefully designed to eliminate any structural/ acoustic resonance with the cavity underneath the slotted plate by designing the walls of the cavity to be sufficiently thick and the size of the cavity to be suitably larger than the acoustic wavelength in the medium. Thus, the flow field observed in this configuration is purely hydrodynamic and represents the evolution of a shear layer over a slotted plate independent of any coupling processes.

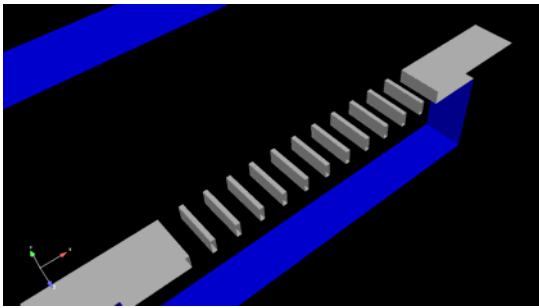


Figure 17. A schematic of the slotted plate configuration studied by Dr. Rockwell and co-workers.

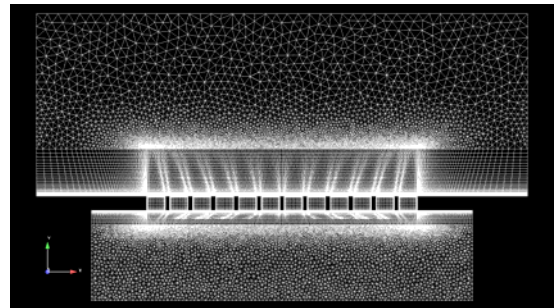


Figure 18. Computational mesh used in the simulations of the slotted plate configuration.

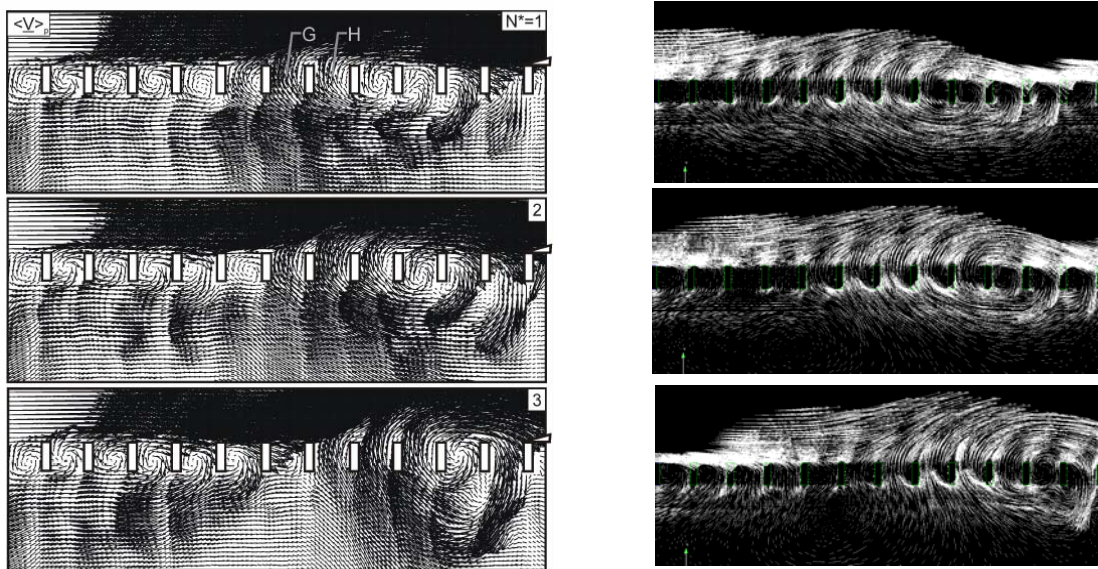


Figure 19. Flow vectors obtained from experiments (left column) and the simulations for the slotted plate configuration.

The experimental measurement consisted of planar imaging of the flow using a cinema technique of high density particle image velocimetry to obtain a sequence of images of quantitative flow parameters over the entire plane. The observations of the flow field indicated that the flow field was largely two-dimensional. Hence, in the simulations a periodic boundary condition was imposed in the spanwise direction. This enabled the reduction of the cost associated with the calculation. The mesh used in these calculations is shown in Figure 18.

A comparison of the flow vectors computed and obtained from the experiments is shown in Figure 19. The experimental vectors are phase averaged, while the CFD vectors are instantaneous vector plots. It is clearly seen that the CFD plots capture all the characteristics seen in the experimental plots. The large scale rollup, the upward flow in the slots upstream of the vortex core, the downward flow in the slots downstream of the vortex core and the circular flow patterns in the slots near the vortex core are all seen to be captured in the CFD plots. The amplitude of the fluctuations in the velocity, as judged by the deflection of the free stream is slightly over-predicted in the calculations. This is potentially due to the restricted spanwise domain used in the calculations. The rate of downstream movement of the vortex core, characteristic of the convection speeds in the shear layer, is also seen to be captured very well in the CFD plots.

A time series of the evolution of the flow field in terms of the velocity vectors and the vertical velocity through the slots is shown in Figure 20. Despite the lack of resonance, the similarities with the flow field in the slot region of the slotted opening resonator (shown in Figure 16) are obvious. A wave, the length of the opening is seen, with the node in this wave corresponding to the core of the large scale vortex. The slots in the region upstream of the vortex core are seen to have large vertical velocities out of the cavity, while the slots in the region downstream of the core have large negative velocities into the cavity. The slots in the middle, close to the core of the large scale vortex are seen to have a self contained rotating flow within each of them. Thus the slot flows themselves oscillate in phase with the propagation of the large scale wave through the opening. Even in the slots well upstream of the main vortex, as the next vortex evolves, the slot flow fields are seen to be in phase with the larger wave evolution. This phase relationship is critical to the behavior of this flow field – any interruptions with this phase relationships is bound to curb the development of the large scale vortex. The similarity with the resonator flow field is indicative of the potential for control of the resonator by interfering with the phase relationships in the system.

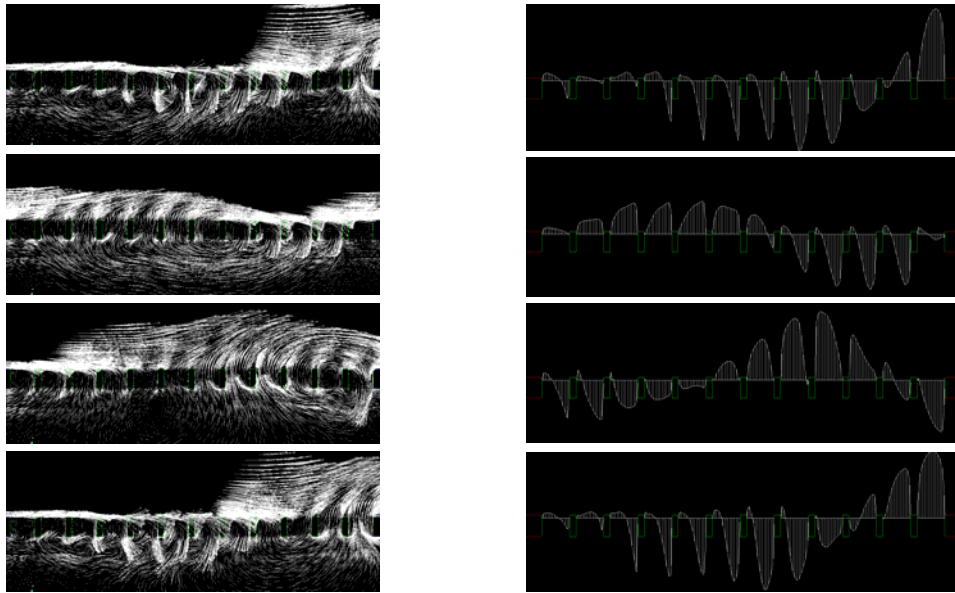


Figure 20. Time series of evolution of the velocity vectors (left hand side column) and the slot vertical velocities (right hand side column) in the slotted plate configuration.

VII. Conclusions and Future Work

The studies presented here have successfully demonstrated the ability of the CRUNCH CFD[®] flow solver to simulate Helmholtz resonator flow fields.

The simulations showed that the enhancements and improvements made to the basic numerical methods in CRUNCH CFD[®] were significant in simulating the various physics issues associated with the Helmholtz resonator. The interplay between the dissipation arising from the basic numerical scheme, gradient limiting technique and the

turbulence model was captured, with the effect of each one of these parameters identified explicitly. Comparisons with experimentally measured Reynolds stress profiles showed that the combination of low dissipation scheme, low dissipation limiter and a hybrid RANS-LES model was the optimal framework for the simulation of these flow fields. Using these parameters, the dependence of the occurrence of resonance on the velocity of the flow was well captured with the predictions of the cavity wall pressure spectra agreeing well with the experimental measurements.

This signifies the availability of a unique tool to study these flow fields and design potential concepts to mitigate the onset of resonance in these flows. Preliminary calculations of some control attempts already existing in the literature were also carried out to demonstrate this feasibility. Simulations were conducted of a configuration consisting of rectangular slats in the opening of the baseline resonator and another configuration consisting of incompressible flow past a slotted plate. These two simulations showed considerable similarities in the physical processes involved in these flows, despite the purely hydrodynamic nature of the incompressible flow field and the presence of resonance in the Helmholtz resonator. This showed that considerable understanding of the processes governing the shear layer behavior in Helmholtz resonators can be obtained by studying the hydrodynamics of the shear layer even under non-resonant conditions. It also demonstrated the existence of Phase relationships in the shear layer that represent potential targets to be controlled.

Our future efforts will be focused on extending the applications of the solver to larger scale configurations. Further underwater configurations will require the use of structural deflection model to capture the flow field dynamics. These two issues will be main focus of the near future efforts.

VIII. Acknowledgments

This material is based upon work supported by the Naval Sea Systems Command under Contract No. N00024-04-C-4165. Any opinions, findings and conclusion or recommendations expressed in this material are those of the author (s) and do not necessarily reflect the views of the Naval Sea Systems command. The contract monitor was Dr. Paul Zoccola, NSWC CD. His contributions are gratefully acknowledged. In addition, valuable discussions with Dr. Ted Farabee and Dr. Joseph Slomski of NSWC CD are also gratefully acknowledged. The meshes for the Helmholtz resonator were provided us by Dr. Slomski for which we are thankful to him. Dr. Donald Rockwell, Professor, Lehigh University, served as a consultant on this effort. He and Mr. A. Cagri Sever provided us material for the simulations of the slotted plate flowfield for which we are thankful to them.

IX. References

- ¹ Arunajatesan, S. and Sinha, N., "Hybrid RANS-LES Modeling for Cavity Aeroacoustics Predictions," *International Journal of Aeroacoustics*, Vol. 2, No. 1, pp 65-91, 2003.
- ² Arunajatesan, S., Shipman, J.D. and Sinha, N., "Hybrid RANS-LES Simulation of Cavity Flowfields with Control," Paper No. AIAA-2002-1130, 40th AIAA Aerospace Sciences Meeting and Exhibit, Reno, NV, January 14-17, 2002.
- ³ Arunajatesan, S., Shipman, J.D., Sinha, N., and Seiner, J.M., "Mechanisms In High-Frequency Control Of Cavity Flows," Paper No. AIAA-2003-0005, 41st AIAA Aerospace Conference & Exhibit, Reno, NV, Jan. 6-9, 2003.
- ⁴ Sinha, N. and Arunajatesan, S., and Ukeiley, L., "High Fidelity Simulation Of Weapons Bay Aeroacoustics Attenuation Using Active Flow Control," Paper No. AIAA-2000-1968, 6th AIAA/CEAS Aeroacoustics Conference, Lahaina, Hawaii, June 12-14, 2000.
- ⁵ C.W.Rowley, T. Colonius and A.J. Basu, "On Self-Sustained Oscillations in Two-Dimensional Compressible Flow Over Rectangular Cavities," *J. Fluid Mech.*, 455: 315-346, 2002.
- ⁶ Sinha, N., York, B.J., Dash, S.M., Chidambaram, N., and Findlay, D., "A Perspective on the Simulation of Cavity Aeroacoustics," AIAA Paper 98-0286, 36th AIAA Aerospace Sciences Meeting, Reno, NV, January 12-15, 1998.
- ⁷ Speziale, C.G., "On Nonlinear K-1 and K- ϵ Models of Turbulence," *J. Fluid Mech.*, Vol. 178, pp. 459-475.
- ⁸ Howe, M.S. 1998 "Acoustics of Fluid-Structure Interaction," Cambridge University Press, Cambridge.
- ⁹ Nelson, P.A., Halliwell, N. and Doak, P.E. "Fluid Dynamics of a Flow-Excited Resonance. Part II: Flow-Acoustic Interaction. The Dissipation of Sound at an Edge" *Journal of Sound and Vibration*, 90, pp.375-402, 1983
- ¹⁰ Hosangadi, A., Lee, R.A., York, B.J., Sinha, N. and Dash, S.M., "Upwind Unstructured Scheme for Three-Dimensional Combusting Flows," *Journal of Propulsion and Power*, Vol. 12, No. 3, pp. 494-503, May-June 1996.
- ¹¹ Arunajatesan, S., Shipman, J.D. and Sinha, N., "Numerical Modeling of Coupled VSTOL-Ship Airwake Flow Fields", HT-FED2004-56147, Proceedings of FEDSM'04, 2004 ASME Heat Transfer/Fluids Engineering Summer Conference, Charlotte, NC, July 11-13, 2004.
- ¹² Barth, T.J., and Linton, S.W., "An Unstructured Mesh Newton Solution for Compressible Fluid Flow and Its Parallel Implementation," AIAA 95-0221, 33rd AIAA Aerospace Sciences Meeting and Exhibit, Reno, NV, January, 1995.
- ¹³ Zoccola, P.J., "Effect of opening obstructions on the flow-excited response of a Helmholtz resonator", *Journal of Fluids and Structures*, V. 19, Issue 7, Pages 1005-1025, August 2004.
- ¹⁴ Rockwell, D., Lin, J.-C., Oshkai, P., Reiss, M., Pollack, M., "Shallow Cavity Flow Tone Experiments: Onset of Locked-on States", *Journal of Fluids and Structures*, Vol. 17, pp 381-414, 2003.